

1 Detection of slow slip events using wavelet
2 analysis of GNSS recordings

3 Ariane Ducellier¹, Kenneth C. Creager², and David A. Schmidt²

4 ¹Corresponding author. University of Washington, Department of
5 Earth and Space Sciences, Box 351310, 4000 15th Avenue NE
6 Seattle, WA 98195-1310

7 ²University of Washington, Department of Earth and Space
8 Sciences

9 **Key points**

- 10 • We use a wavelet-based signal processing method to detect transients in
11 GNSS data, such as slow slip events.
- 12 • There is a good correlation between detections of slow slip using GNSS
13 data and using tremor data.
- 14 • The method could be applied in regions where no tremor is detected in
15 conjunction with slow slip events.

₁₆ **Abstract**

₁₇ In many places, tectonic tremor is observed in relation to slow slip and can
₁₈ be used as a proxy to study slow slip events of moderate magnitude where
₁₉ surface deformation is hidden in Global Navigation Satellite System (GNSS)
₂₀ noise. However, in subduction zones where no clear relationship between tremor
₂₁ and slow slip occurrence is observed, these methods cannot be applied, and we
₂₂ need other methods to be able to better detect and quantify slow slip. Wavelets
₂₃ methods such as the Discrete Wavelet Transform (DWT) and the Maximal
₂₄ Overlap Discrete Wavelet Transform (MODWT) are mathematical tools for
₂₅ analyzing time series simultaneously in the time and the frequency domain by
₂₆ observing how weighted differences of a time series vary from one period to the
₂₇ next. In this paper, we use wavelet methods to analyze GNSS time series and
₂₈ seismic recordings of slow slip events in Cascadia. We use detrended GNSS
₂₉ data, apply the MODWT transform and stack the wavelet details over several
₃₀ nearby GNSS stations. As an independent check on the timing of slow slip
₃₁ events, we also compute the cumulative number of tremor in the vicinity of the
₃₂ GNSS stations, detrend this signal, and apply the MODWT transform. In both
₃₃ time series, we can then see simultaneous waveforms whose timing corresponds
₃₄ to the timing of slow slip events. We assume that there is a slow slip event
₃₅ whenever there is a positive peak followed by a negative peak in the wavelet
₃₆ signal. We verify that there is a good correlation between slow slip events
₃₇ detected with only GNSS data, and slow slip events detected with only tremor
₃₈ data for northern Cascadia. The wavelet-based detection method detects well
₃₉ events of magnitude higher than 6 as determined by independent event catalogs
₄₀ (e.g. [Michel et al., 2019]).

41 **1 Introduction**

42 Slow slip events are a new feature discovered in the last two decades in many
43 subduction zones thanks to recordings of the displacement of Earth's surface by
44 dense Global Navigation Satellite System (GNSS) networks [Vergnolle et al.,
45 2010, Schmidt and Gao, 2010, Jiang et al., 2012, Wallace et al., 2012]. As with
46 ordinary earthquakes, slow slip events represent slip on a fault, for instance
47 the plate boundary between a tectonic plate subducting under another tectonic
48 plate. However, they take a much longer time (several days to several years) to
49 happen relative to ordinary earthquakes. They have a relatively short recurrence
50 time (months to years) compared to the recurrence time of regular earthquakes
51 (up to several hundreds of years), allowing scientists to observe and study many
52 complete event cycles, which is typically not possible to explore with traditional
53 earthquake catalogs [Beroza and Ide, 2011]. A slow slip event on the plate
54 boundary is inferred to happen when there is a reversal of the direction of mo-
55 tion at GNSS stations, compared to the secular interseismic motion. Slow slip
56 events have been observed in many places [Beroza and Ide, 2011, Audet and
57 Kim, 2016], such as Cascadia [Bartlow, 2020], Nankai [Nishimura et al., 2013],
58 Alaska [Li et al., 2016], Costa Rica [Jiang et al., 2012], Mexico [Radiguet
59 et al., 2012], and New Zealand [Wallace, 2020].

60

61 In many places, tectonic tremor is also observed in relation to slow slip, but
62 it is more abundant in some places [Hall et al., 2018]. Tremor is a long (several
63 seconds to many minutes), low amplitude seismic signal, with emergent onsets,
64 and an absence of clear impulsive phases. Tectonic tremor have been explained
65 as a swarm of small, low-frequency earthquakes (LFEs) [Shelly et al., 2007],
66 which are small magnitude earthquakes ($M \sim 1$) for which frequency content
67 (1-10 Hz) is lower than for ordinary earthquakes (up to 20 Hz). In subduction

68 zones such as Nankai and Cascadia, tectonic tremor observations are spatially
69 and temporally correlated with slow slip observations [Obara, 2002, Rogers
70 and Dragert, 2003]. Due to this correlation, these paired phenomena have been
71 called Episodic Tremor and Slip (ETS). However, this is not always the case.
72 For instance, in northern New Zealand, tremor is more challenging to detect,
73 and seems to be located downdip of the slow slip on the plate boundary [Todd
74 and Schwartz, 2016]. In Alaska, the tremor zone only partially overlaps the
75 long-term slow slip zone and there does not appear to be any temporal correla-
76 tion between tremor and slow slip occurrence [Wech, 2016].

77

78 In Cascadia, there are robust signals in both GNSS and tremor [Hawthorne
79 and Rubin, 2013]. This is also the case in Nankai [Hiramatsu et al., 2008], where
80 tiltmeters are used instead of GNSS. It is thus possible to use tremor as a proxy
81 to observe slow slip events that are not directly observed in the GNSS data.
82 For instance, Aguiar et al. [2009] studied 23 ETS events in Cascadia with more
83 than 50 hours of tectonic tremor. For all these events, they computed both the
84 GPS-estimated moment release and the cumulative number of hours of tectonic
85 tremor recorded. They observed a linear relationship between moment release
86 and number of hours of tremor for ETS events of moment magnitude 6.3 to 6.8.
87 Based on this linear relationship, it is possible to infer the existence of smaller
88 slow slip events of magnitude 5-6 occurring simultaneously with smaller tremor
89 bursts of duration 1 to 50 hours occurring in between the big ETS events, and
90 for which there is no detectable signal in the GPS data.

91

92 Frank [2016] divided GPS time series observations from Cascadia and Guer-
93 rero, Mexico, into two groups: the first group contains days with abundant
94 tremor and LFEs, the second group contains days when the number of tremor

95 or LFEs is lower than a threshold. He then stacked separately the two groups
96 of daily observations and observed a cumulative displacement in the direction
97 corresponding to the loading period when few tremor or LFEs are observed
98 and the surface deformation corresponds to the secular plate motion. He also
99 observed a cumulative displacement in the opposite direction corresponding to
100 the release period when tremor and LFEs are observed. He was thus able to
101 observe a reverse displacement corresponding to smaller slow slip events not
102 directly observable in the GPS data for individual events.

103

104 However, these methods cannot be applied to detect slow slip events in places
105 where tremor and slow slip occurrence are not well spatially and temporally cor-
106 related, tremor is not abundant, or the seismic network is not robust enough.
107 We thus need other methods to be able to better detect and quantify slow slip.

108

109 Wavelet methods such as the Discrete Wavelet Transform (DWT) are math-
110 ematical tools for analyzing time series simultaneously in the time and the fre-
111 quency domain by observing how weighted differences of a time series vary from
112 one period to the next. Wavelet methods have been widely used for geophysical
113 applications (e.g. Kumar and Foufoula-Georgiou [1997]). However, few studies
114 have used wavelet methods to analyze recordings of slow slip, and their scope
115 was limited to the detection of the bigger (magnitude 6-7) short-term (a few
116 weeks) events [Szeliga et al., 2008, Ohtani et al., 2010, Wei et al., 2012, Alba
117 et al., 2019].

118

119 Szeliga et al. [2008] determined the timing and the amplitude of 34 slow
120 slip events throughout the Cascadia subduction zone between 1997 and 2005
121 using wavelets. They modeled the GPS time series by the sum of a linear trend,

122 annual and biannual sinusoids representing seasonal effects, Heaviside step func-
123 tions corresponding to earthquakes and hardware upgrades, and a residual sig-
124 nal. They then applied a Gaussian wavelet transform to the residual time series
125 to get the exact timing of slow slip at each GPS station. The idea is that the
126 wavelet transform allows us to analyze the signal both in the time and the fre-
127 quency domains. A sharp change in the signal will be localized and seen at all
128 levels of the wavelet decomposition, contrary to what happens with the periodic
129 sinusoids of the Fourier transform.

130

131 Instead of using wavelets in the time domain, Ohtani et al. [2010] used 2D
132 wavelet functions in the spatial domain to detect slow slip events. They de-
133 signed the Network Stain Filter (NSF) to detect transient deformation signals
134 from large-scale geodetic arrays. They modeled the position of the GPS station
135 by the sum of the secular velocity, a spatially coherent field, site-specific noise,
136 reference frame errors, and observation errors. The spatial displacement field is
137 modeled by the sum of basis wavelets with time-varying weights. Their method
138 has been successfully used to detect a transient event in the Boso peninsula,
139 Japan, and a slow slip event in the Alaska subduction zone [Wei et al., 2012].

140

141 Finally, Alba et al. [2019] used hourly water level records from four tide
142 gauges in the Juan de Fuca Straight and the Puget Sound to determine rela-
143 tive vertical displacements associated with ETS events between 1996 and 2011.
144 Their main idea is that the tidal level measured at a given gauge is the sum of
145 a noise component at multiple timescales (tides, ocean and atmospheric noise)
146 and an uplift signal due to the ETS events. The noise component is assumed to
147 be coherent between all tidal gauges, while the tectonic uplift signal is different
148 provided that the gauges are far enough from each other. By stacking the tidal

149 records after removing tides, the uplift signals cancel each other while the noise
150 signal is amplified. By stacking the details of the DWT decomposition, instead
151 of stacking the raw tidal record, each of the components of the noise at different
152 time scales is retrieved and can then be removed from the raw records to obtain
153 the uplift signal. The authors were then able to clearly see a difference in uplift
154 between the two tidal gauges at Port Angeles and Port Townsend.

155

156 In our study, we use a similar approach to previous studies with a different
157 reasoning. We only stack signals at nearby GPS stations, assuming that the
158 longitudinal displacement due to the ETS events will then be the same at each
159 of the GPS stations considered. We suppose that some of the noise component
160 is different at each GPS station and will be eliminated by the stacking. Fi-
161nally, we assume that the noise and the longitudinal displacement due to the
162 ETS events and the secular plate motion have different time scales, so that the
163 wavelet decomposition will act as a bandpass filter to retrieve the displacement
164 signal and highlight the ETS events. We use wavelet methods to analyze GPS
165 and tremor recordings of slow slip events in Cascadia. Our objective is to verify
166 that there is a good correlation between slow slip events detected with only
167 GNSS data, and slow slip events detected with only tremor data. We thus want
168 to demonstrate that the wavelet-based detection method can be applied to de-
169tect slow slip events that may currently be obscured using standard methods.

170

171 2 Data

172 We focused our study on northwest Washington State. For the GNSS data, we
173 used the GPS time series provided by the Pacific Northwest Geodetic Array,
174 Central Washington University. These are network solutions in ITRF2008 with

175 phase ambiguities resolved. Solutions are computed with JPL/NASA orbits and
176 satellite clocks. North, East, and Vertical directions are available. However, as
177 the direction of the secular plate motion is close to the East direction, we only
178 used the East direction of the GPS time series for the data analysis, as it has
179 the best signal-to-noise ratio. The wavelet method works best with data with
180 zero mean, and no sharp discontinuities; so we use the cleaned dataset, that is
181 GPS times series with linear trends, steps due to earthquakes or hardware up-
182 grades, and annual and semi-annual sinusoids signals simultaneously estimated
183 and removed following Szeliga et al. [2004]. For the tremor data, we used the
184 tremor catalog from the Pacific Northwest Seismic Network (PNSN) [Wech,
185 2010].

186

187 **3 Method**

188 **3.1 The Maximal Overlap Discrete Wavelet Transform**

189 The Discrete Wavelet Transform (DWT) is an orthonormal transform that
190 transforms a time series X_t ($t = 0, \dots, N - 1$) into a vector of wavelet coeffi-
191 cients W_i ($i = 0, \dots, N - 1$). If we denote J the level of the wavelet decompo-
192 sition, and the number of observations is equal to $N = n * 2^J$, where n is some
193 integer higher or equal to 1, the vector of wavelet coefficients can be decomposed
194 into J wavelet vectors W_j of lengths $\frac{N}{2}, \frac{N}{4}, \dots, \frac{N}{2^J}$, and one scaling vector V_J
195 of length $\frac{N}{2^J}$. Each wavelet vector W_j is associated with changes on time scale
196 $\tau_j = dt2^{j-1}$, where dt is the time step of the time series, and corresponds to the
197 filtering of the original time series with a filter with nominal frequency interval
198 $[\frac{1}{dt2^{j+1}}; \frac{1}{dt2^j}]$. The scaling vector V_J is associated with averages in time scale
199 $\lambda_J = dt2^J$, and corresponds to the filtering of the original time series with a

200 filter with nominal frequency interval $[0; \frac{1}{dt2^{j+1}}]$. Wavelet vectors can be further
 201 decomposed into details and smooths, which are more easily interpretable. We
 202 define for $j = 1, \dots, J$ the j th wavelet detail D_j , which is a vector of length
 203 N , and is associated to time scale $\tau_j = dt2^{j-1}$. Similarly, we can define for
 204 $j = 1, \dots, J$ the j th wavelet smooth S_j , which is a vector of length N , and is
 205 associated to scales $\tau_{j+1} = dt2^{j+1}$ and higher. The basic idea is to reapply to
 206 W_j the wavelet filter that was used to construct W_j from the initial time series
 207 X . Together, the details and the smooths define the multiresolution analysis
 208 (MRA) of X :

$$X = \sum_{j=1}^J D_j + S_J \quad (1)$$

210 The DWT presents several disadvantages. First, the length of the time se-
 211 ries must be a multiple of 2^J where J is the level of the DWT decompositon.
 212 Second, the time step of the wavelet vector W_j is $dt2^j$, which may not corre-
 213 spond to the time when some interesting phenomenon is visible on the original
 214 time series. Third, when we circularly shift the time series, the corresponding
 215 wavelet coefficients, details and smooths are not a circularly shifted version of
 216 the wavelet coefficients, details and smooths of the original time series. Thus,
 217 the values of the wavelet coefficients, details and smooths are strongly dependent
 218 on the time when we start experimentally gathering the data. Finally, when we
 219 filter the time series to obtain the details D_j and smooths S_j , we introduce a
 220 phase shift, which makes it difficult to line up meaningfully the features of the
 221 MRA with the original time series.

222

223 To overcome the disadvantages described above, we use instead the Maxi-
 224 mal Overlap Discrete Wavelet Transform (MODWT). The MODWT transforms
 225 the time series X_t ($t = 0, \dots, N - 1$) into J wavelet vectors \widetilde{W}_j ($j = 1, \dots, J$) of

226 length N and a scaling vector \tilde{V}_J of length N . As is the case for the DWT,
 227 each wavelet vector \tilde{W}_j is associated with changes on scale $\tau_j = dt2^{j-1}$, and
 228 corresponds to the filtering of the original time series with a filter with nominal
 229 frequency interval $[\frac{1}{dt2^{j+1}}; \frac{1}{dt2^j}]$. The scaling vector \tilde{V}_J is associated with aver-
 230 ages in scale $\lambda_J = dt2^J$, and corresponds to the filtering of the original time
 231 series with a filter with nominal frequency interval $[0; \frac{1}{dt2^{j+1}}]$. As is the case for
 232 the DWT, we can write the MRA:

$$233 \quad X = \sum_{j=1}^J \tilde{D}_j + \tilde{S}_J \quad (2)$$

234 The MODWT of a time series can be defined for any length N . The time
 235 step of the wavelet vectors \tilde{W}_j and the scaling vector \tilde{V}_J is equal to the time
 236 step of the original time series. When we circularly shift the time series, the
 237 corresponding wavelet vectors, scaling vector, details and smooths are shifted
 238 by the same amount. The details and smooths are associated with a zero phase
 239 filter, making it easy to line up meaningfully the features of the MRA with the
 240 original time series. The wavelet methods for time series analysis are explained
 241 in a more detailed way in [Percival and Walden, 2000]).
 242

243 **3.2 Application to synthetic data**

244 To illustrate the wavelet transform method, we first apply the MODWT to syn-
 245 thetic data. As slow slip events occur in Cascadia on a regular basis, every
 246 twelve to eighteen months, we create a synthetic signal of period $T = 500$ days.
 247 To reproduce the ground displacement observed on the longitudinal component
 248 of GPS stations in Cascadia, we divide each period into two parts: In the first
 249 part of duration $T - N$, the displacement is linearly increasing and corresponds
 250 to the inter seismic plate motion in the eastern direction; in the second part

251 of duration N , the displacement is linearly decreasing and corresponds to a
252 slow slip event on a reverse fault at depth triggering a ground displacement in
253 the western direction. To see the effect of the duration of the slow slip event,
254 we use different values for $N = 5, 10, 20, 40$ days. The amplitude of the set is
255 normalized to 1. Figure 1 shows the synthetics, the details D_j of the wavelet
256 decomposition for levels 1 to 10, and the smooth S_{10} for the four durations of a
257 slow slip event.

258

259 The ramp-like signal is transformed through the wavelet filtering into a wave-
260 form with first a positive peak and then a negative peak. The shape of the wave-
261 form is the same for every level of the wavelet decomposition, but the width of
262 the waveform increases with the scale level. For the 8th level of the wavelet de-
263 composition, the width of the waveform is nearly as large as the time between
264 two events. At larger scales, the waveforms start to merge two contiguous events
265 together, and make the wavelet decomposition less interpretable. For an event
266 of duration 5 days, the wavelet details at levels higher than 3 have a larger
267 amplitude than the wavelet details at lower scales. For an event of duration 10
268 days, the wavelet details at levels higher than 4 have a larger amplitude than
269 the wavelet details at lower scales. For an event of duration 20 days, the wavelet
270 details at levels higher than 5 have a larger amplitude than the wavelet details
271 at lower scales. For an event of duration 40 days, the wavelet details at levels
272 higher than 6 have a larger amplitude than the wavelet details at lower scales.
273 Thus, the scale levels at which an event is being seen in the wavelet details give
274 us an indication about the duration (and the magnitude) of the slow slip event.
275 The big slow slip events of magnitude 6-7 typically trigger a signal that lasts
276 about one week at an individual GPS station, and the whole event lasts several
277 weeks. We expect them to start being visible at the level 5 of the wavelet de-

278 composition, but to not be noticeable at lower time scales.

279

280 3.3 MODWT of GPS and tremor data

281 The DWT and MODWT methods must be used on a continuous time series,
282 without gaps in the recordings. To deal with the gaps in the GNSS recordings,
283 we simply replace the missing values by interpolation. The value for the first
284 day for which data are missing is equal to the mean of the five days before
285 the gap. The value for the last day for which data are missing is equal to the
286 mean of the five days after the gap. The remaining missing values are com-
287 puted by doing a linear interpolation of the first and the last values and adding
288 a Gaussian noise component with mean zero and standard deviation equal to
289 the standard deviation of the whole time series. The straight line starts at and
290 ends at . We verify how the wavelet details may be affected by looking at a GPS
291 time series without missing values and compared the wavelet details with and
292 without removing some data points. Station PGC5 recorded continuous 1390
293 days between 2009 and 2013 without any missing values. We first computed
294 the wavelet details without missing values. Then, we removed ten neighboring
295 values, replaced them using the method described above (linear interpolation
296 plus Gaussian noise), and computed the wavelet details with the replaced val-
297 ues. Figure 2 shows a comparison of the two wavelet details for two different
298 locations of the missing values. We can see that there are visible differences
299 in the time series itself, and in the details at the smallest levels of the wavelet
300 decomposition. However, the differences between the wavelet details with and
301 without missing values get smaller and smaller with increasing levels of details,
302 and are barely visible for the levels that are most relevant (levels 6 and above).
303 We thus conclude that we can easily replace the missing values in the GNSS

304 time series without introducing false detections of slow slip events.

305

306 We then applied the wavelet filtering to real GPS data. Figure 3 shows the
307 longitudinal displacement for GPS station PGC5, located in southern Vancou-
308 ver Island, the details of the wavelet decomposition for levels 1 to 8, and the
309 smooth. In the data, we can see a sharp drop in displacement whenever there is
310 a documented slow slip event. For levels 5 to 8, which correspond to time scales
311 16, 32, 64 and 128 days, we can see in the details a positive peak followed by
312 a negative peak whenever there is a drop in displacement in the data. We thus
313 verify that the wavelet method can detect steps in the time series associated
314 with slow slip events.

315

316 To increase the signal-to-noise ratio and better detect slow slip events, we
317 stack the signal from several neighboring GPS stations. We choose to focus on
318 GPS stations located close enough to the tremor zone to get a sufficiently high
319 amplitude of the slow slip signal. We choose 16 points along the 40 km depth
320 contour of the plate boundary (model from Preston et al. [2003]) with spacing
321 equal 0.1 degree in latitude (red triangles on Figure 4). Then we took all the
322 GPS stations located in a 50 km radius for a given point, compute the wavelet
323 details for the longitudinal displacement of each station, and stack each detail
324 over the GPS stations. We thus have a stacked detail for each level 1 to 10 of
325 the wavelet decomposition.

326

327 To assess the success of the wavelet decomposition for detecting slow slip
328 events in GPS time series, we validate the approach by comparing to an inde-
329 pendent proxy for ETS events. We took all the tremor epicenters located within
330 a 50 km radius centered on one of the 16 locations marked by red triangles on

331 Figure 3. Then we computed the cumulative number of tremor within this
332 circle. Finally, we removed a linear trend from the cumulative tremor count,
333 and applied the wavelet transform. Figure 5 shows an example of the wavelet
334 decomposition for the third northernmost location on Figure 4 (which is closest
335 to GPS station PGC5). Contrary to what happens for the GPS data, we see
336 a sharp increase in the time series whenever there is a tremor episode, which
337 translates into a negative peak followed by a positive peak in the wavelet details.

338 4 Results

339 We stacked the 8th level detail of the wavelet decomposition of the displacement
340 over all the GPS stations located in a 50 km radius of a given point, for the 16
341 locations indicated in Figure 3. The result is shown in the top panel of Figure 6,
342 where each line represents one of the locations along strike. To better highlight
343 the peaks in the wavelet details, we highlighted in red the time intervals where
344 the amplitude of the stacked detail is higher than a threshold, and in blue the
345 time intervals where the amplitude of the stacked detail is lower than minus the
346 threshold. To compare the GPS signal with the tremor signal, we plotted the
347 8th level detail of the wavelet decomposition of the tremor count on the bottom
348 panel of Figure 6. We multiplied by -1 the cumulative tremor count for the
349 wavelet decomposition in order to be able to match positive peaks with positive
350 peaks and negative peaks with negative peaks. In the tremor catalog from the
351 PNSN, there are 17 tremor events with more than 150 hours of tremor recorded.
352 The events are summarized in Table 1. The time of the event is the start date
353 plus half the duration of the event.

354

355 Although the latitudinal extension of the events is not always the same for
356 the GPS data and for the tremor data, we identify the same 13 events in both 8th

357 wavelet decompositions for the 8th level: January 2007, May 2008, May 2009,
358 August 2010, August 2011, September 2012, September 2013, August-November
359 2014, January 2016, March 2017, June 2018, March-November 2019, and Oc-
360 tober 2020-January 2021. Although there are two events in the tremor catalog
361 in August 2014 and November 2014, these two events are not distinguishable in
362 the 8th level details and look more like a single event slowly propagating from
363 South to North. The same phenomenon is observed in 2019 when two tremor
364 events in March and November 2019 are merged into a single event propagating
365 slowly from South to North. In 2020-2021, the wavelet decomposition of the
366 tremor shows one event in the south in October-November 2020 and one event
367 in the North in January 2021, but in the wavelet decomposition of the GPS
368 data, these three events look like a single event propagating slowly from South
369 to North.

370

371 A similar comparison is shown for the wavelet decomposition of the GPS
372 data and the wavelet decomposition of the tremor count data for the 7th level
373 and the 6th level respectively (Figures 7 and 8). The events are harder to see in
374 the 7th level than in the 8th level, both for the GPS data and the tremor count
375 data. The wavelet decomposition is more noisy for the GPS data between 2010
376 and 2012, but it does not seem that there are more slow slip events visible in
377 the 7th level.

378

379 For the 6th level detail, we see an additional event in the South in Fall 2009
380 that is present both in the GPS and the tremor data. It may correspond to the
381 northern extent of a big ETS event occurring in Fall 2009 south of the study
382 area (event 19 in the Michel et al. [2019] catalog). There are three small sig-
383 nals in the GPS data in Winter 2012, Fall 2017, and Winter 2020 that are not

384 present in the tremor data, and may be false detections. To summarize, we
 385 assume that true detections are events present in both GPS and tremor time
 386 series, and false detections are events present in the GPS but not in the tremor
 387 time series. Then, all the 13 events present on the 8th level detail of the wavelet
 388 decomposition are true detections and 14 of the 17 events present on the 6th
 389 level detail of the wavelet decomposition are true detections.

390

391 5 Discussion

392 To better evaluate the number of true and false detections, we convert the
 393 wavelet details into binary time series. If the absolute value of the wavelet
 394 detail is higher than a threshold, we replace the value by 1 (for positive values)
 395 or -1 (for negative values), otherwise we replace the value by 0. We do this
 396 on both the wavelet details of the GPS data and of the tremor data. Then we
 397 decide that if both the GPS and the tremor time series take the value 1 (or
 398 both take the value -1), we have a true detection (true positive, TP). If the
 399 GPS and the tremor time series have opposite signs, or if the absolute value of
 400 the GPS time series is 1 but the value of the tremor time series is 0, we have a
 401 false detection (false positive, FP). If both time series take the value 0, we do
 402 not have detection (true negative, TN). If the GPS time series take the value
 403 0, but the absolute value of the tremor time series is 1, we miss a detection
 404 (false negative, FN). We then define the sensitivity (true positive rate) and the
 405 specificity (equal to 1 minus the false positive rate) as:

$$\begin{aligned}
 \text{sensitivity} &= \frac{TP}{TP + FN} \\
 \text{specificity} &= \frac{TN}{TN + FP}
 \end{aligned} \tag{3}$$

406 We can then evaluate the quality of the detections obtained with our method
407 by plotting a receiver operating characteristic curve (ROC curve). The ROC
408 curve is widely use for binary classification problems in statistics and machine
409 learning. We calculate an ROC value by varying the values of the threshold
410 (here the two thresholds used to convert the GPS and the tremor time series
411 into binary time series), computing the corresponding values of the true positive
412 rate and the false positive rate (equal to 1 minus the specificity), and plotting
413 the true positive rate as a function of the false positive rate. If the classifica-
414 tion was made randomly, all the points would fall on the first diagonal. If the
415 classifier was perfect, the corresponding point would fall on the top left cor-
416 ner of the graph with true positive rate equal to 1 and false positive rate equal
417 to 0. The bigger the area under the curve, the better the classification method is.

418

419 As the slow slip events are better seen on levels 6, 7 and 8 of the wavelet
420 decomposition, we first add the wavelet details corresponding to levels 6 to 8,
421 and transform the resulting time series into a binary time series. We apply this
422 transform to both the GPS and the tremor time series with varying thresholds.
423 We then plot the ROC curve on Figure 9, each dot representing a different
424 threshold. The corresponding sums of the wavelet details for the GPS data and
425 the tremor data are shown on Figure 10. We can see that there is a trade-off
426 between sensitivity and specificity as we vary the threshold. If we decrease the
427 false positive rate, we also decrease the number of true events detected. If we
428 increase the number of true events detected, we also increase the false positive
429 rate. In Figure 10, we have chosen thresholds for the GPS time series and the
430 tremor time series such that the specificity is higher than 0.75, and the sensitiv-
431 ity is the highest possible, that is we have chosen the thresholds corresponding
432 to the dot that is farthest from the diagonal, which is random.

433

434 In addition to the magnitude 6 events discussed above, Michel et al. [2019]
435 have also identified several magnitude 5 events using a variational Bayesian In-
436 dependent Component Analysis (vbICA) decomposition of the signal. As we
437 expect smaller magnitude events to be more visible at smaller time scales of
438 the wavelet decomposition (level 5), we verify for all these events whether a
439 signal can be seen at the same time as the time given in their catalog. Most
440 of these magnitude 5 events are also sub-events of bigger magnitude 6 events.
441 Table 2 summarizes for each event its timing, its number and its magnitude as
442 indicated in the catalog from Michel et al. [2019], and whether it is part of a
443 bigger magnitude 6 event. Figure 11 shows the 5th level detail wavelet decom-
444 position of the GPS data. Red lines show the timing of the big ETS events from
445 Table 1, and blue lines show the timing of the small slow slip events from Table 2.

446

447 All 14 events that are sub-events of a bigger event are visible at level 5.
448 However, this may be because the bigger events are clearly seen at levels 6 to 8,
449 and also at smaller time scales. The one small event that is not part of a bigger
450 event (Winter 2009) is visible at level 5 of the wavelet decomposition. However,
451 some other events that are not in the catalog of Michel et al. [2019]’s catalog
452 are also visible in late 2007, early 2010, early 2012, and late 2016. Therefore,
453 it is difficult to differentiate between a true detection and a false detection, and
454 to conclude whether the method can indeed detect events of magnitude 5.

455

456 In Figure 9, we see four smaller events that are not in the catalog of Michel
457 et al. [2019]: at about 2007.5, there is a negative peak followed by a positive peak
458 (that is an event in the opposite direction of what would be expected from slow
459 slip), at about 2010.2, 2012.2 and 2020.2, there are positive peaks followed by

460 negative peaks for all the sixteen locations studied in this paper. Looking back
461 at the original GPS data, there is a small increase in the displacement in the
462 eastern direction that lasts about one or two months at about 2007.5. However,
463 the direction of the displacement does not correspond to a slow slip event, and
464 another cause should be found to explain this signal. There is a decrease in
465 displacement that lasts several months at about 2010.2. This transient may
466 correspond to a long duration slow slip event. There is a small decrease in
467 displacement at about 2012.2. Its amplitude is small but the duration and
468 direction correspond to a slow slip event, so this transient could be a very small
469 slow slip event. Finally, there is also a small decrease in displacement at about
470 2020.2 that is difficult to interpret.

471 6 Conclusion

472 In this paper, we develop and test a new approach for detecting transient events
473 in GPS time series, such as slow slip events. We used wavelet methods to an-
474alyze GNSS time series and tremor recordings of slow slip events in Cascadia.
475 We used detrended GNSS data, applied the MODWT transform, and stacked
476 the wavelet details over several nearby GNSS stations. As an independent check
477 on the timing of slow slip events, we also computed the cumulative number of
478 tremor in the vicinity of the GNSS stations, detrended this signal, and applied
479 the MODWT transform. In both time series, we could then see simultaneous
480 waveforms whose timing corresponds to the timing of slow slip events. We as-
481sumed that there is a slow slip event whenever the wavelet signal gets above
482 a threshold. We verified that there is a good correlation between slow slip
483 events detected with only GNSS data, and slow slip events detected with only
484 tremor data. The wavelet-based detection method detects all events of magni-
485tude higher than 6 as determined by independent event catalogs (e.g. [Michel

486 et al., 2019]). We detected signals in the GPS data that could be magnitude
487 5 events, but it is not easy to differentiate between true detections and false
488 detections.

489 Data and Resources

490 The GPS recordings used for this analysis can be downloaded from the PANGA
491 website [GPS/GNSS Network and Geodesy Laboratory: Central Washington
492 University, other/seismic network, 1996] <http://www.panga.cwu.edu/>. The
493 Python scripts used to analyze the data and make the figures can be found
494 on the first author's Github account <https://github.com/ArianeDucellier/>
495 `slowlip`. Figure 4 was created using GMT [Wessel and Smith, 1991].

496 Acknowledgements

497 This work was funded by the grant from the National Science Foundation EAR-
498 1358512. A.D. would like to thank Professor Donald Percival for introducing
499 her to wavelet methods during his excellent class on Wavelets: Data Analysis,
500 Algorithms and Theory taught at University of Washington.

501 Declaration of Competing Interests

502 The authors declare no competing interests.

503 References

504 A.C. Aguiar, T.I. Melbourne, and C.W. Scrivner. Moment release rate of Cas-
505 cadia tremor constrained by GPS. *J. Geophys. Res.*, 114:B00A05, 2009.

- 506 S. Alba, R. J. Weldon, D. Livelybrooks, and D. A. Schmidt. Cascadia ETS
507 events seen in tidal records (1980–2011). *Bull. Seismol. Soc. Am.*, 109(2):
508 812–821, 2019.
- 509 P. Audet and Y.H. Kim. Teleseismic constraints on the geological environment
510 of deep episodic slow earthquakes in subduction zone forearcs: A review.
511 *Tectonophysics*, 670:1–15, 2016.
- 512 N. M. Bartlow. A longterm view of episodic tremor and slip in Cascadia. *Geo-*
513 *physical Research Letters*, 43(3):e2019GL085303, 2020.
- 514 G.C. Beroza and S. Ide. Slow earthquakes and nonvolcanic tremor. *Annu. Rev.*
515 *Earth Planet. Sci.*, 39:271–296, 2011.
- 516 W.B. Frank. Slow slip hidden in the noise: The intermittence of tectonic release.
517 *Geophys. Res. Lett.*, 43:10125–10133, 2016.
- 518 GPS/GNSS Network and Geodesy Laboratory: Central Washington University,
519 other/seismic network. Pacific Northwest Geodetic Array (PANGA), 1996.
520 URL <http://www.panga.cwu.edu/>.
- 521 K. Hall, H. Houston, and D. Schmidt. Spatial comparisons of tremor and slow
522 slip as a constraint on fault strength in the northern Cascadia subduction
523 zone. *Geochemistry, Geophysics, Geosystems*, 19(8):2706–2718, 2018.
- 524 J. C. Hawthorne and A. M. Rubin. Shorttime scale correlation between slow
525 slip and tremor in Cascadia. *Journal of Geophysical Research: Solid Earth*,
526 118:1316–1329, 2013.
- 527 Y. Hiramatsu, T. Watanabe, and K. Obara. Deep lowfrequency tremors as a
528 proxy for slip monitoring at plate interface. *Geophysical Research Letters*, 35:
529 L13304, 2008.

- 530 Y. Jiang, S. Wdowinski, T. H. Dixon, M. Hackl, M. Protti, and V. Gonzalez.
531 Slow slip events in Costa Rica detected by continuous GPS observations,
532 2002-2011. *Geochemistry, Geophysics, Geosystems*, 13:Q04006, 2012.
- 533 P. Kumar and E. Foufoula-Georgiou. Wavelet analysis for geophysical applica-
534 tions. *Rev. Geophys.*, 35(4):385–412, 1997.
- 535 S. Li, J. Freymueller, and R. McCaffrey. Slow slip events and timedeependent
536 variations in locking beneath Lower Cook Inlet of the AlaskaAleutian sub-
537 duction zone. *Journal of Geophysical Research: Solid Earth*, 121:1060–1079,
538 2016.
- 539 S. Michel, A. Gualandi, and J.-P. Avouac. Interseismic coupling and slow slip
540 events on the Cascadia megathrust. *Pure Appl. Geophys.*, 176:3867–3891,
541 2019.
- 542 T. Nishimura, T. Matsuzawa, and K. Obara. Detection of shortterm slow slip
543 events along the Nankai Trough, southwest Japan, using GNSS data. *Journal*
544 *of Geophysical Research: Solid Earth*, 118:3112–3125, 2013.
- 545 K. Obara. Nonvolcanic deep tremor associated with subduction in southwest
546 Japan. *Science*, 296(5573):1679–1681, 2002.
- 547 R. Ohtani, J.J. McGuire, and P. Segall. Network strain filter: A new tool for
548 monitoring and detecting transient deformation signals in GPS arrays. *J.*
549 *Geophys. Res.*, 115:B12418, 2010.
- 550 D.B. Percival and A.T. Walden. *Wavelet Methods for Time Series Analysis*.
551 Cambridge Series in Statistical and Probabilistic Mathematics. Cambridge
552 University Press, New York, NY, USA, 2000.
- 553 L.A. Preston, K.C. Creager, R.S. Crosson, T.M. Brocher, and A.M. Trehu.

- 554 Intraslab earthquakes: Dehydration of the Cascadia slab. *Science*, 302:1197–
555 1200, 2003.
- 556 M. Radiguet, F. Cotton, M. Vergnolle, M. Campillo, A. Walpersdorf, N. Cotte,
557 and V. Kostoglodov. Slow slip events and strain accumulation in the Guerrero
558 gap, Mexico. *Journal of Geophysical Research: Solid Earth*, 117:B04305, 2012.
- 559 G. Rogers and H. Dragert. Tremor and slip on the Cascadia subduction zone:
560 The chatter of silent slip. *Science*, 300(5627):1942–1943, 2003.
- 561 D. A. Schmidt and H. Gao. Source parameters and timedeependent slip distribu-
562 tions of slow slip events on the Cascadia subduction zone from 1998 to 2008.
563 *Journal of Geophysical Research: Solid Earth*, 115:B00A18, 2010.
- 564 D.R. Shelly, G.C. Beroza, and S. Ide. Non-volcanic tremor and low-frequency
565 earthquake swarms. *Nature*, 446:305–307, 2007.
- 566 W. Szeliga, T.I. Melbourne, M.M. Miller, and V.M. Santillan. Southern Casca-
567 dia episodic slow earthquakes. *Geophys. Res. Lett.*, 31:L16602, 2004.
- 568 W. Szeliga, T. Melbourne, M. Santillan, and M. Miller. GPS constraints on 34
569 slow slip events within the Cascadia subduction zone, 1997-2005. *J. Geophys.*
570 *Res.*, 113:B04404, 2008.
- 571 E.K. Todd and S.Y. Schwartz. Tectonic tremor along the northern Hikurangi
572 Margin, New Zealand, between 2010 and 2015. *J. Geophys. Res. Solid Earth*,
573 121:8706–8719, 2016.
- 574 M. Vergnolle, A. Walpersdorf, V. Kostoglodov, P. Tregoning, J. A. Santiago,
575 N. Cotte, and S. I. Franco. Slow slip events in Mexico revised from the
576 processing of 11 year GPS observations. *Journal of Geophysical Research:*
577 *Solid Earth*, 115:B08403, 2010.

- 578 L. M. Wallace. Slow slip events in New Zealand. *Annual Review of Earth and*
579 *Planetary Sciences*, 48:175–203, 2020.
- 580 L. M. Wallace, J. Beavan, S. Bannister, and C. Williams. Simultaneous longterm
581 and shortterm slow slip events at the Hikurangi subduction margin, New
582 Zealand: Implications for processes that control slow slip event occurrence,
583 duration, and migration. *Journal of Geophysical Research: Solid Earth*, 117:
584 B11402, 2012.
- 585 A.G. Wech. Interactive tremor monitoring. *Seismol. Res. Lett.*, 81(4):664–669,
586 2010.
- 587 A.G. Wech. Extending Alaska’s plate boundary; tectonic tremor generated by
588 Yakutat subduction. *Geology*, 44(7):587–590, 2016.
- 589 M. Wei, J.J. McGuire, and E. Richardson. A slow slip event in the south central
590 Alaska Subduction Zone. *Geophys. Res. Lett.*, 39:L15309, 2012.
- 591 P. Wessel and W. H. F. Smith. Free software helps map and display data. *EOS*
592 *Trans. AGU*, 72:441, 1991.

⁵⁹³ **Addresses**

⁵⁹⁴ Ariane Ducellier. University of Washington, Department of Earth and Space
⁵⁹⁵ Sciences, Box 351310, 4000 15th Avenue NE Seattle, WA 98195-1310.

⁵⁹⁶

⁵⁹⁷ Kenneth C. Creager. University of Washington, Department of Earth and
⁵⁹⁸ Space Sciences, Box 351310, 4000 15th Avenue NE Seattle, WA 98195-1310.

⁵⁹⁹

⁶⁰⁰ David A. Schmidt. University of Washington, Department of Earth and
⁶⁰¹ Space Sciences, Box 351310, 4000 15th Avenue NE Seattle, WA 98195-1310.

602 Tables

Table 1: Episodic Tremor and Slip events with $M \geq 6$ identified by MODWT in both the GPS and the tremor data. The duration and the number of tremor are from the tremor catalog of the PNSN. The event number and the magnitude are from the slow slip catalog of Michel et al. [2019].

Time	Duration (days)	Number of tremor (hours)	Event number	Magnitude
2007.06	28	398	3	6.68
2008.36	25	402	10	6.56
2009.35	24	248	16	6.49
2010.63	29	518	24	6.54
2011.60	37	479	30	6.47
2012.72	37	620	34	6.54
2013.71	27	423	41	6.58
2014.65	15	190	48	6.03
2014.89	38	385	51	6.40
2016.11	43	421	54	6.79
2017.23	19	279	59	6.61
2018.49	22	381		
2019.23	34	195		
2019.88	16	205		
2020.79	26	193		
2020.86	12	162		
2021.09	14	230		

Table 2: Magnitude 5 events from Michel et al. [2019].

Time	Event number	Magnitude	Sub-event of bigger event
2007.06	1	5.64	Yes
2007.08	2	5.91	Yes
2008.38	11	5.50	Yes
2009.16	14	5.50	No
2009.36	17	5.32	Yes
2010.63	25	5.76	Yes
2011.66	31	5.61	Yes
2011.66	32	5.32	Yes
2012.69	35	5.56	Yes
2013.74	42	5.71	Yes
2014.69	49	5.31	Yes
2014.93	52	5.39	Yes
2016.03	57	5.80	Yes
2017.13	60	5.43	Yes
2017.22	61	5.37	Yes

603 **Figure captions**

- 604 • Figure 1. Demonstration of a wavelet decomposition for a synthetic dataset.
605 A synthetic time series is created (top row) with steps of period 500 days,
606 and transient durations of 2 days (left), 5 days, 10 days, and 20 days
607 (right). The resulting details and smooths are shown in increasing level.
608 The amplitude of the synthetic time series is normalized to 1, and the
609 details and smooths show the relative amplitude.
- 610 • Figure 2. Top: Data from GPS station PGC5 without missing values
611 (black) and with missing values replaced by the sum of a straight line and
612 a Gaussian noise component (red) for two locations of the missing values
613 (left and right). The corresponding ten details and smooths of the wavelet
614 composition are shown in increasing levels for the original data (black) and
615 for the missing values replaced by linear interpolation plus Gaussian noise
616 (red).
- 617 • Figure 3. Top: Longitudinal displacement recorded at GPS station PGC5.
618 The resulting details and smooth of the wavelet decomposition are shown
619 in increasing level.
- 620 • Figure 4. GPS stations used in this study (black triangles). The black
621 line represents the 40 km depth contour of the plate boundary model by
622 Preston et al. [2003]. The red triangles are the locations where we stack
623 the GPS data. The small grey dots are all the tremor locations from the
624 PNSN catalog.
- 625 • Figure 5. Details and smooth of the wavelet decomposition of the de-
626 trended cumulative tremor count around the third northernmost red tri-
627 angles on Figure 3 (latitude 48.5).

- Figure 6. Top: Stacked 8th level details of the wavelet decomposition of the displacement over all the GPS stations located in a 50 km radius of a given point, for the 16 red triangles indicated in Figure 3. Bottom: 8th level detail multiplied by -1 of the cumulative tremor count in a 50 km radius of a given point for the same 16 locations. The black lines represent the timings of the ETS events from Table 1. We mark by a red rectangle every time where the amplitude is higher than a threshold of 0.4 (for the GPS) or 0.003 (for the tremor). We mark by a blue rectangle every time where the amplitude is lower than minus the threshold.
- Figure 7. Same as Figure 6 but for the 7th level detail. The thresholds are 0.5 (for the GPS) and 0.01 (for the tremor).
- Figure 8. Same as Figure 6 but for the 6th level detail. The thresholds are 0.3 (for the GPS) and 0.009 (for the tremor).
- Figure 9. Same as Figure 6 but for the sum of the 6th, 7th and 8th level details. The thresholds are 0.8 (for the GPS) and 0.01 (for the tremor).
- Figure 10. ROC curve for the sum of the 6th, 7th, and 8th level details of the wavelet decomposition. Each black dot represents the true positive rate of event detections and the false positive rate of event detections for a given pair of thresholds (for the GPS and for the tremor). The red cross marks the true positive rate and the false positive rate obtained with the thresholds used to make Figure 9.
- Figure 11. Top: Stacked 5th level details of the wavelet decomposition of the displacement over all the GPS stations located in a 50 km radius of a given point, for the 16 red triangles indicated in Figure 3. The red lines represent the timings of the ETS events from Table 1. The blue

653 lines represent the timings of the magnitude 5 events from the catalog of
654 Michel et al. [2019].

655 **Figures**

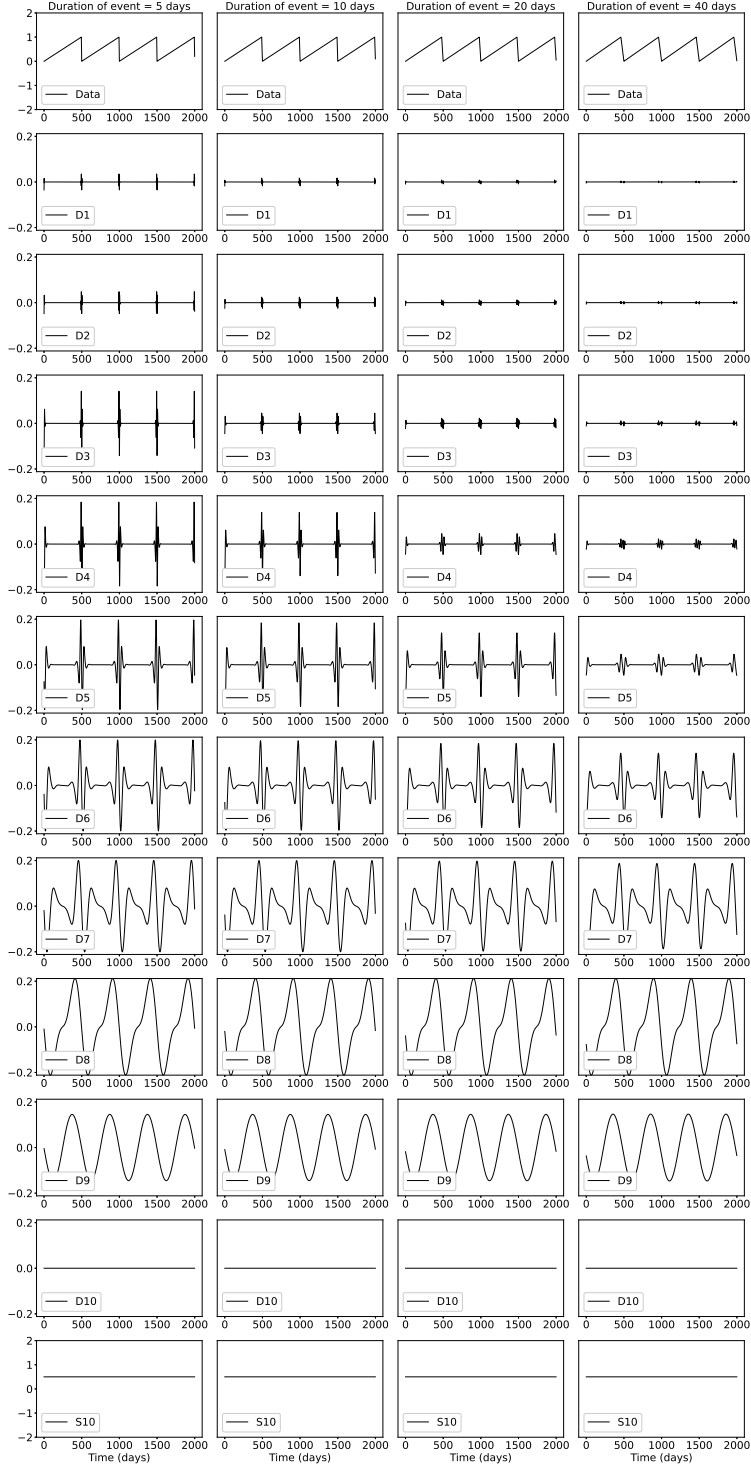


Figure 1: Demonstration of a wavelet decomposition for a synthetic dataset. A synthetic time series is created (top row) with steps of period 500 days, and transient durations of 2 days (left), 5 days, 10 days, and 20 days (right). The resulting details and smooths are shown in increasing level. The amplitude of the synthetic time series is normalized to 1, and the details and smooths show the relative amplitude.

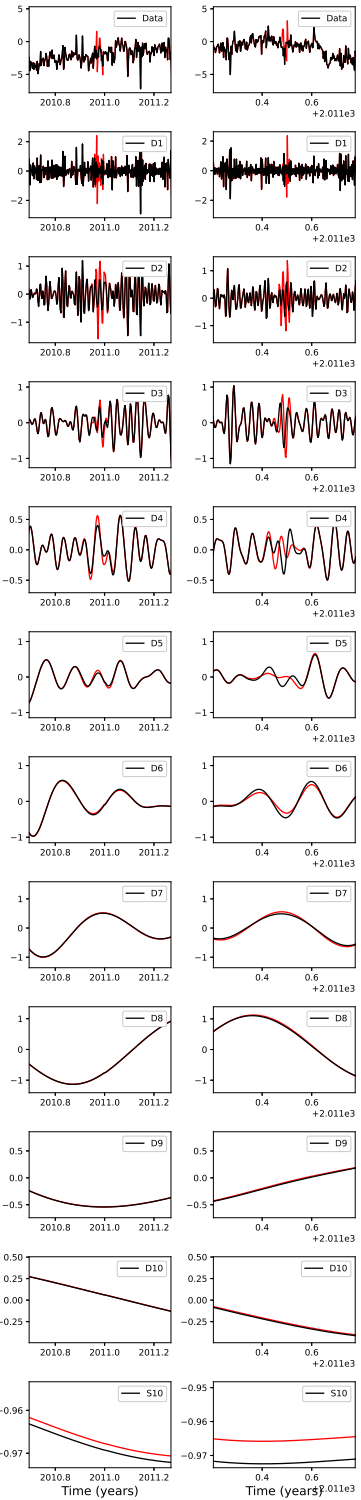


Figure 2: Top: Data from GPS station PGC5 without missing values (black) and with missing values replaced by the sum of a straight line and a Gaussian noise component (red) for two locations of the missing values (left and right). The corresponding ten details and smooths of the wavelet composition are shown in increasing levels for the original data (black) and for the missing values replaced by linear interpolation plus Gaussian noise (red).

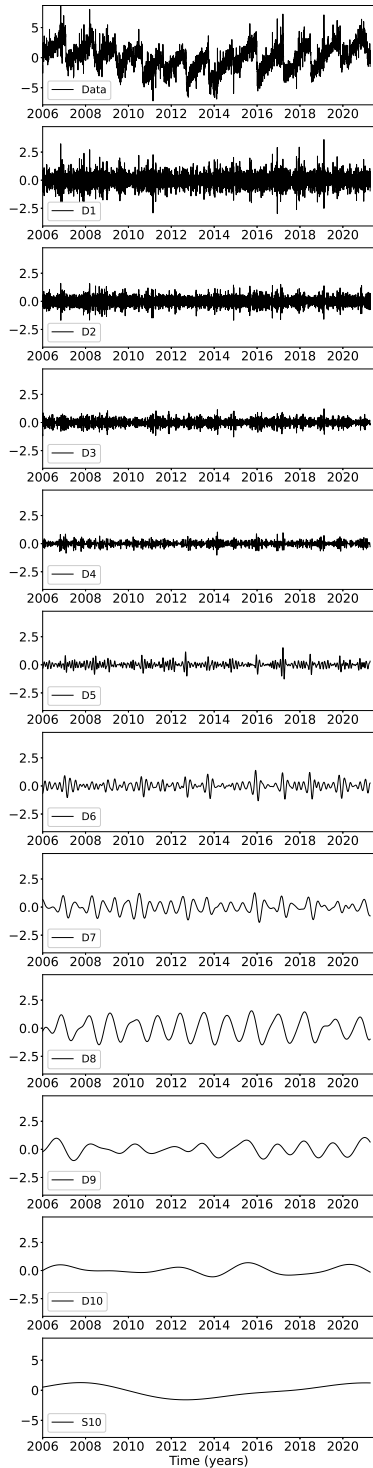


Figure 3: Top: Longitudinal displacement recorded at GPS station PGC5. The resulting details and smooth of the wavelet decomposition are shown in increasing level.

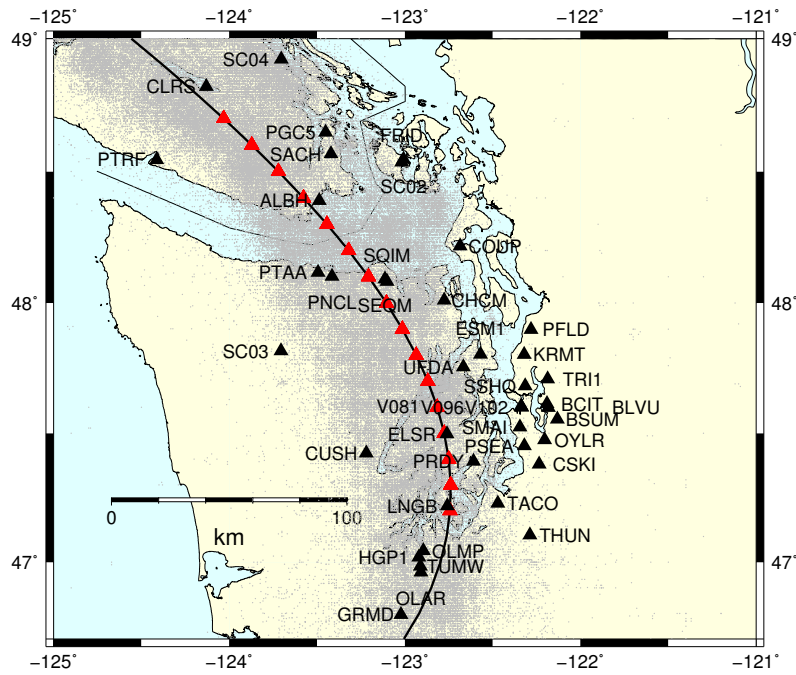


Figure 4: GPS stations used in this study (black triangles). The black line represents the 40 km depth contour of the plate boundary model by Preston et al. [2003]. The red triangles are the locations where we stack the GPS data. The small grey dots are all the tremor locations from the PNSN catalog.

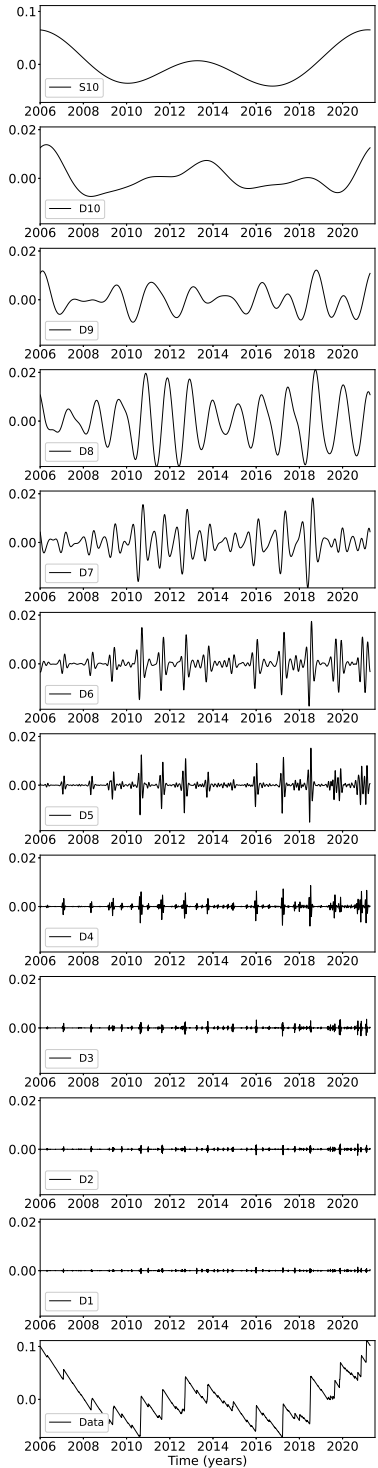


Figure 5: Details and smooth of the ³³wavelet decomposition of the detrended cumulative tremor count around the third northernmost red triangles on Figure 3 (latitude 48.5).

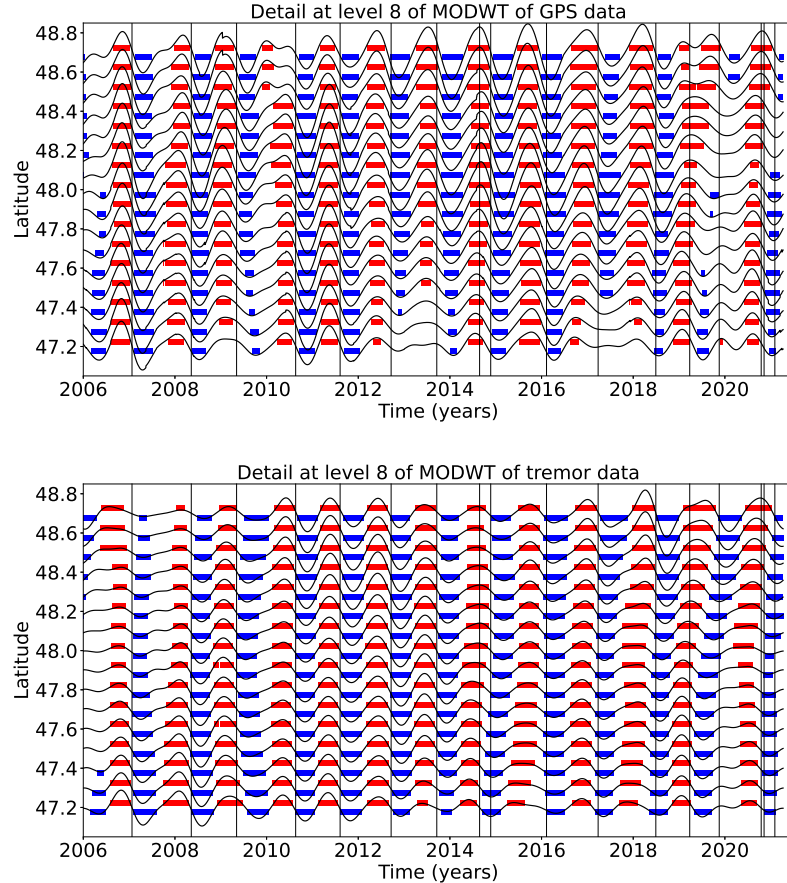


Figure 6: Top: Stacked 8th level details of the wavelet decomposition of the displacement over all the GPS stations located in a 50 km radius of a given point, for the 16 red triangles indicated in Figure 3. Bottom: 8th level detail multiplied by -1 of the cumulative tremor count in a 50 km radius of a given point for the same 16 locations. The black lines represent the timings of the ETS events from Table 1. We mark by a red rectangle every time where the amplitude is higher than a threshold of 0.4 (for the GPS) or 0.003 (for the tremor). We mark by a blue rectangle every time where the amplitude is lower than minus the threshold.

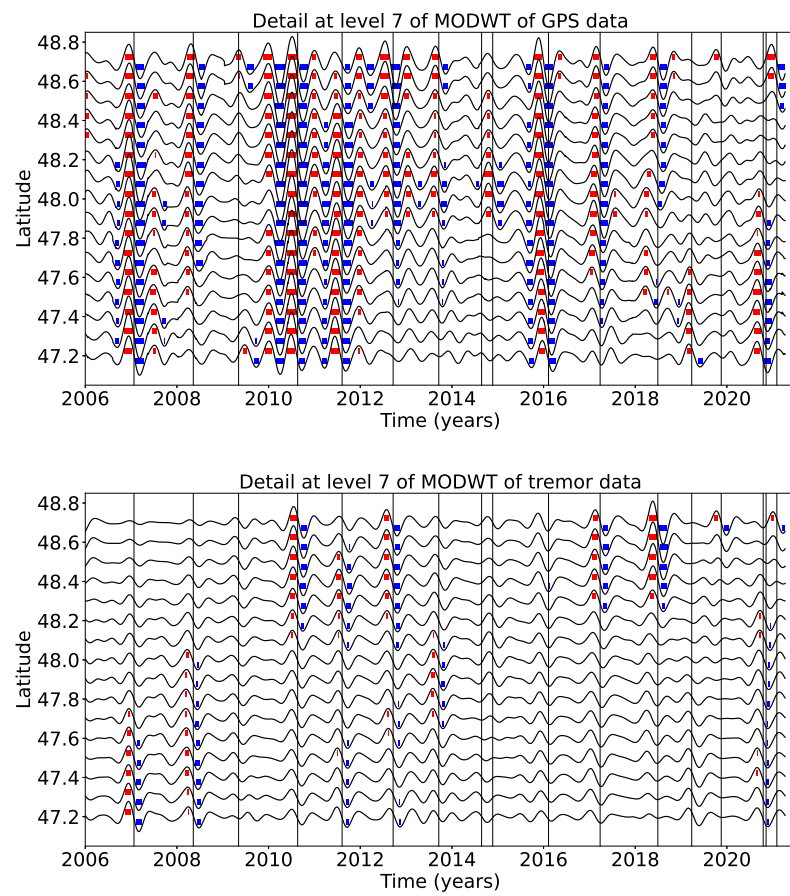


Figure 7: Same as Figure 6 but for the 7th level detail. The thresholds are 0.5 (for the GPS) and 0.01 (for the tremor).

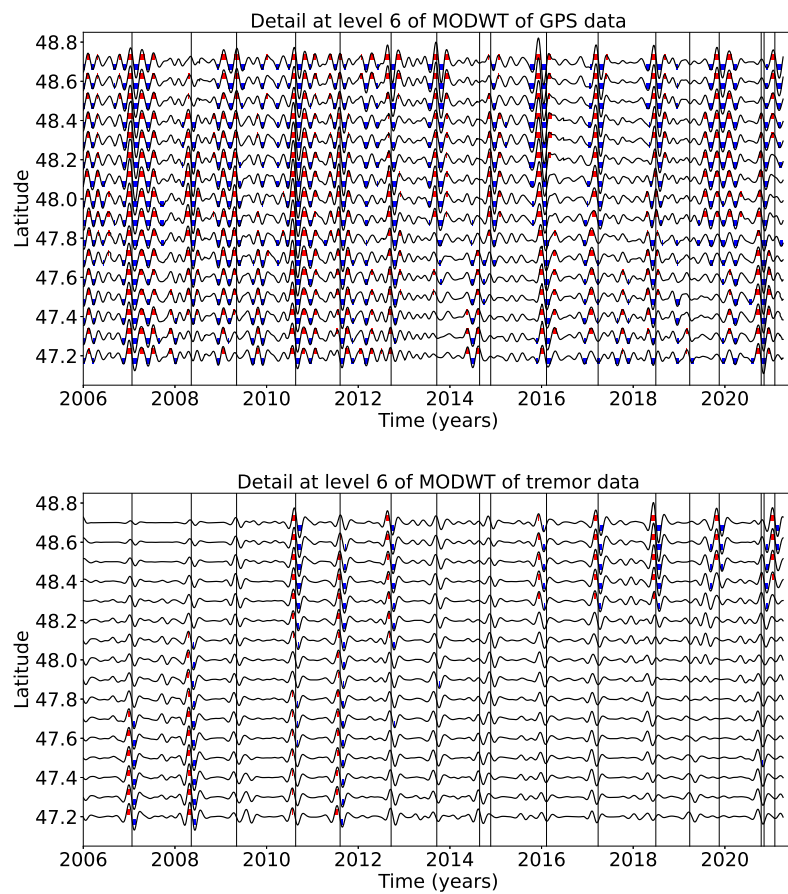


Figure 8: Same as Figure 6 but for the 6th level detail. The thresholds are 0.3 (for the GPS) and 0.009 (for the tremor).

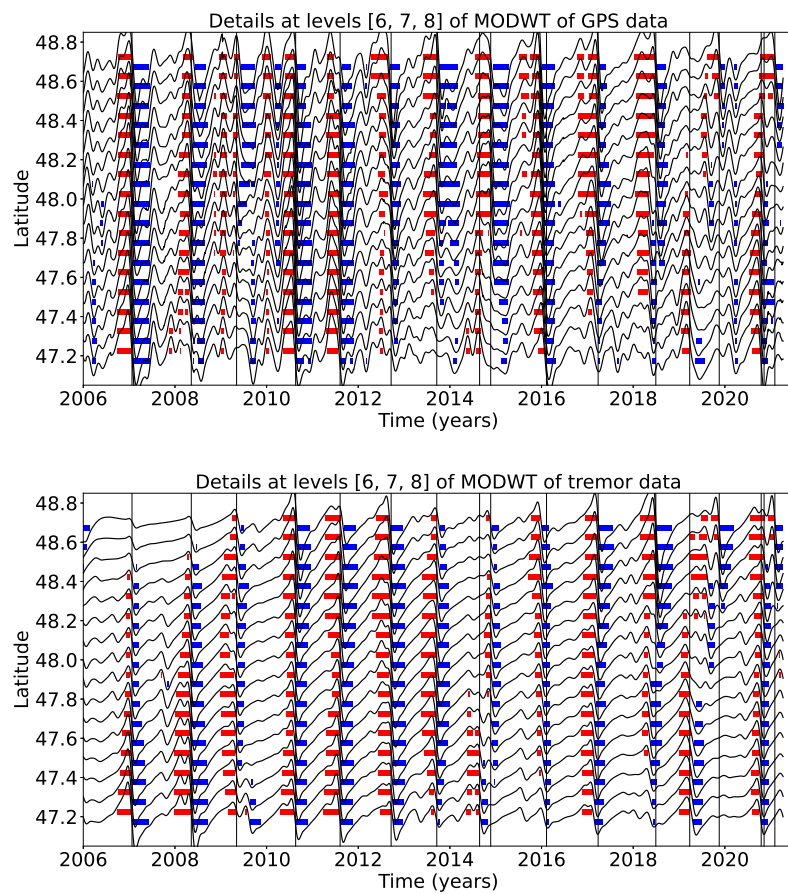


Figure 9: Same as Figure 6 but for the sum of the 6th, 7th and 8th level details. The thresholds are 0.8 (for the GPS) and 0.01 (for the tremor).

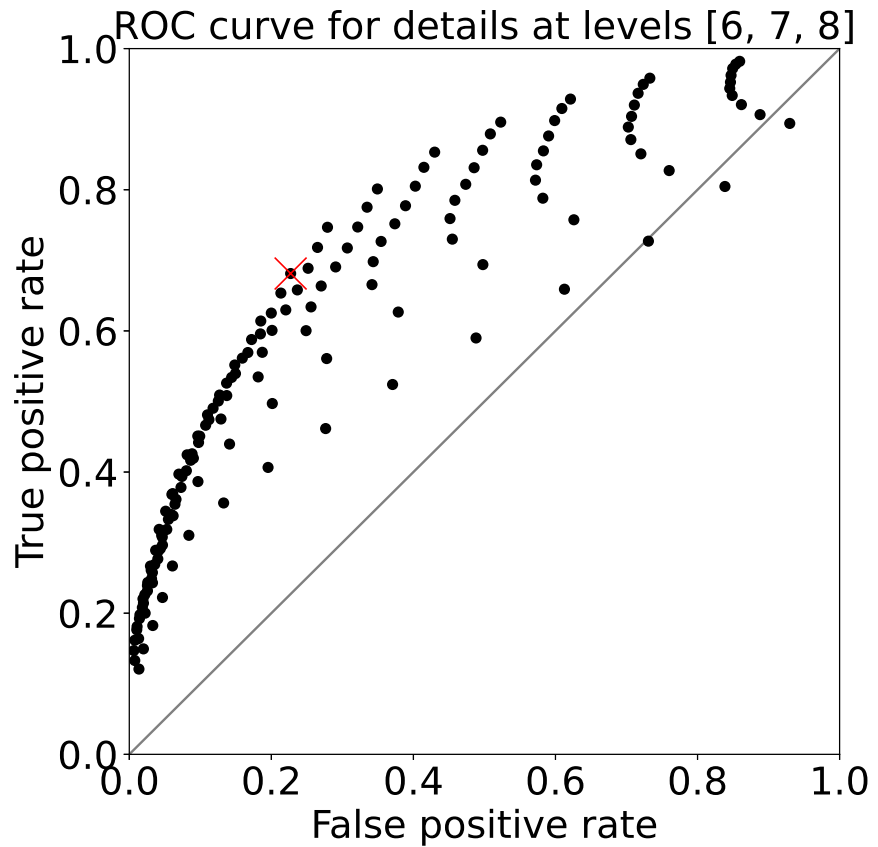


Figure 10: ROC curve for the sum of the 6th, 7th, and 8th level details of the wavelet decomposition. Each black dot represents the true positive rate of event detections and the false positive rate of event detections for a given pair of thresholds (for the GPS and for the tremor). The red cross marks the true positive rate and the false positive rate obtained with the thresholds used to make Figure 9.

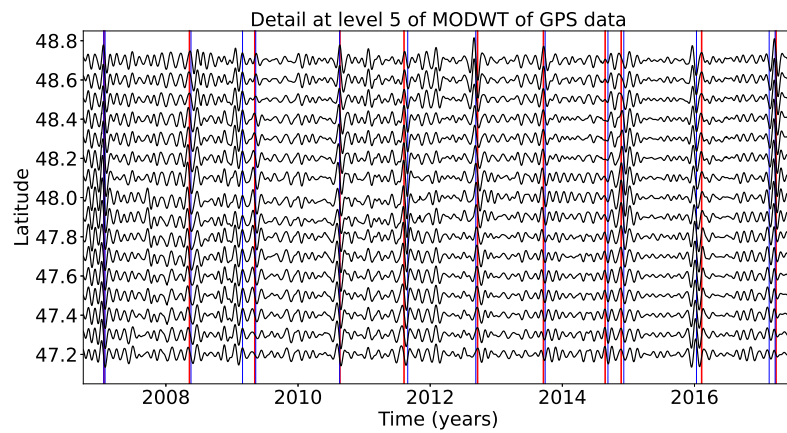


Figure 11: Top: Stacked 5th level details of the wavelet decomposition of the displacement over all the GPS stations located in a 50 km radius of a given point, for the 16 red triangles indicated in Figure 3. The red lines represent the timings of the ETS events from Table 1. The blue lines represent the timings of the magnitude 5 events from the catalog of Michel et al. [2019].